Earth's Future

RESEARCH ARTICLE
10.1029/2020EF001873

Key Points:

- There are robust intermodel correlations across elements of the Southern Ocean climate system in historical Coupled Model Intercomparison Project, Phase 5 (CMIP5) simulations
- The baseline Southern Ocean temperature relationship extends to projected changes in radiation, cloudiness, the jet latitude and sea ice
- CMIP5 models with initially cooler Southern Ocean exhibit more global warming, likely due to greater capacity for change

Correspondence to:
J. B. Kajtar and M. Collins,
jules.kajtar@utas.edu.au;
M.Collins@exeter.ac.uk.

Citation:
Kajtar, J. B., Santoso, A., Collins, M., Taschetto, A. S., England, M. H., & Frankcombe, L. M. (2021). CMIP5 intermodel relationships in the baseline Southern Ocean climate system and with future projections. *Earth's Future*, *9*, e2020EF001873. https://doi.org/10.1029/2020EF001873

Received 22 OCT 2020
Accepted 26 MAY 2021

Author Contributions:
Conceptualization: Jules B. Kajtar, Agus Santoso, Matthew Collins, Matthew H. England
Investigation: Jules B. Kajtar, Agus Santoso
Methodology: Jules B. Kajtar, Agus Santoso, Matthew Collins, Andréa S. Taschetto, Matthew H. England, Leela M. Frankcombe
Project Administration: Jules B. Kajtar, Matthew Collins
Supervision: Matthew Collins

CMIP5 Intermodel Relationships in the Baseline Southern Ocean Climate System and With Future Projections

Jules B. Kajtar[1,2,3], Agus Santoso[3,4,5], Matthew Collins[1], Andréa S. Taschetto[3,4], Matthew H. England[3,4], and Leela M. Frankcombe[3,4]

[1]College of Engineering, Mathematics, and Physical Sciences, University of Exeter, Exeter, UK, [2]Institute for Marine and Antarctic Studies, University of Tasmania, TAS, Australia, [3]Australian Research Council Centre of Excellence for Climate Extremes, ACT, Australia, [4]Climate Change Research Centre, University of New South Wales, Sydney, NSW, Australia, [5]Centre for Southern Hemisphere Oceans Research (CSHOR), CSIRO Oceans and Atmosphere, Hobart, TAS, Australia

Abstract Climate models exhibit a broad range in the simulated properties of the climate system. In the early historical period, the absolute global mean surface air temperature in Coupled Model Intercomparison Project, Phase 5 (CMIP5) models spans a range of ~12°C – 15°C. Other climate variables may be linked to global mean temperature, and so accurate representation of the baseline climate state is crucial for meaningful future climate projections. In CMIP5 baseline climate states, statistically significant intermodel correlations between Southern Ocean surface temperature, outgoing shortwave radiation, cloudiness, the position of the mid-latitude eddy-driven jet, and Antarctic sea ice area are found. The baseline temperature relationships extend to projected future changes in the same set of variables, impacting on the projected global mean surface temperature change. Models with initially cooler Southern Ocean tend to exhibit more global warming, and vice versa for initially warmer models. These relationships arise due to a "capacity for change". For example, cold-biased models tend to have more cloud cover, sea ice, and equatorward jet initially, and thus a greater capacity to lose cloud cover and sea ice, and for the jet to shift poleward under global warming. A first look at emerging data from CMIP6 reveals a shift of the relationship from the Southern Ocean towards the Antarctic region, possibly due to reductions in Southern Ocean biases, such as in westerly wind representation.

Plain Language Summary Modern simulations of the Earth's climate system differ in some of their large-scale features. For example, in models reported on by the Intergovernmental Panel on Climate Change in the Fifth Assessment Report, the global average temperature ranges between 12°C and 15°C. Global mean temperature is known to be linked to other features, such as wind, clouds, and rainfall. Accurately modeling the present-day climate is important, so that we can have more confidence in the possible futures they simulate under different levels of anthropogenic greenhouse gas emissions. In this study, strong relationships are found between simulated Southern Ocean temperature and the amount of sea ice and clouds. In addition, it is found that the initial Southern Ocean temperature is also related to changes in sea ice and cloud simulated in the future. A model that is cooler initially, for example, tends to have more sea ice and cloud, but also loses more sea ice and cloud in the future, and simulates more global warming.

1. Introduction

Accurately gauging the sensitivity of the Earth's climate to greenhouse gas forcing is crucial for efforts to mitigating the risks of human-induced climate change. But the Earth's climate sensitivity remains highly uncertain. The most typical measure, equilibrium climate sensitivity (ECS), is defined as the global temperature change in response to a doubling to atmospheric CO_2. The Intergovernmental Panel on Climate Change estimated a likely range in ECS of 1.5°C – 4.5°C in the Fifth Assessment Report (AR5; Stocker et al., 2013). A more recent review, using multiple lines of evidence, narrowed the range to 2.6°C – 3.9°C (Sherwood et al., 2020).

Writing – original draft: Jules B. Kajtar, Agus Santoso, Matthew Collins, Andréa S. Taschetto, Matthew H. England, Leela M. Frankcombe
Writing – review & editing: Jules B. Kajtar, Agus Santoso, Matthew Collins, Andréa S. Taschetto, Matthew H. England

Climate models of all levels of sophistication have been used to estimate climate sensitivity, but modern efforts focus on the use of general circulation models or Earth system models which include biogeochemical processes. No two climate models are identical, with some exhibiting low sensitivity and others high (e.g., Flato et al., 2013; Forster et al., 2013; Zhai et al., 2015). Furthermore, all models exhibit some level of bias when compared with observational data. One approach to reducing the level of uncertainty in climate sensitivity is that of "emergent constraints" (Hall et al., 2019). Emergent constraints aim to find links between the bias of particular variables in the baseline climate, and their evolution under radiative forcing. If a relationship emerges, across a wide range of different climate models, then the projected range from less biased models may provide a useful constraint on projections (Hall et al., 2019). The emergent constraints approach crucially depends upon drawing from a large number of unique climate models. Increasing availability of such model data, as notably facilitated by the Coupled Model Intercomparison Project (CMIP), allows for deeper studies into the impact of model biases on future projections.

Baseline global mean surface temperature (GMST) has been explored as just one of many possible constraints on climate sensitivity. CMIP, Phase 5 (CMIP5) models exhibit a wide range in long-term averaged absolute GMST over the historical period (~12°C – 15°C; Flato et al., 2013). No statistically significant relationship has been found between baseline temperature and ECS in CMIP5 (Flato et al., 2013), nor with future temperature change (Hawkins & Sutton, 2016), though it has been noted that there is an absence of models with overly warm baseline temperature and strong global warming (Hawkins & Sutton, 2016). Accurately simulating absolute temperature is generally considered less important than, for instance, initializing a model with near-zero net top-of-atmosphere (TOA) energy balance (Hawkins & Sutton, 2016), as temperature projections are typically measured relative to a baseline period (i.e., represented as anomalies).

Past studies have examined possible relationships between elements of the Southern Hemisphere climate system and climate sensitivity. CMIP3 models exhibited a strong relationship between Southern Hemisphere net TOA radiation and climate sensitivity (Trenberth & Fasullo, 2010; their Figure 13). Whilst showing that the intermodel correlation is strong, Trenberth & Fasullo (2010) also acknowledge that the relationship could also be due to other model processes or biases, which might be common across models, and hence the true climate sensitivity cannot be inferred. Grise et al. (2015) find a weaker intermodel correlation between climate sensitivity and Southern Hemisphere net TOA radiation amongst CMIP5 models. They show that the relationship only exists in a subset of CMIP5 models with "unrealistically bright present-day clouds in the Southern Hemisphere sub-tropics"—a characteristic that is typical amongst CMIP3 models (Grise et al., 2015). Thus, the apparent relationship between net TOA radiation and climate sensitivity is not supported by any physical mechanism, and manifests merely as a result of model biases. Southern Ocean cloudiness and net radiation were therefore deemed inappropriate for constraining equilibrium climate sensitivity (Grise et al., 2015).

Despite some processes being poorly represented in models (Hyder et al., 2018), the Southern Ocean is a key component of the global climate system (e.g., Frölicher et al., 2015; Marshall & Speer, 2012; Sarmiento et al., 2004; Toggweiler & Samuels, 1995). Characterized by circumpolar circulation under the influence of the prevalent westerly winds, it plays an important role in the global thermohaline circulation and the uptake of heat and carbon (Manabe et al., 1991; Marshall & Speer, 2012; Mikaloff Fletcher et al, 2006; Toggweiler & Samuels, 1995), which is similarly dominant in CMIP5 models (Frölicher et al., 2015).

In this study, the relationships between baseline variables in the Southern Ocean climate system and their projected changes are explored. A wide range of variables are analyzed together, and intermodel correlations and regressions are computed. Motivated by the emergent constraints approach, and utilizing the complete suite of CMIP5 simulations, we aim to explore the possible role of baseline biases in the Southern Ocean system in CMIP5, and their impact on projected changes, locally and globally. A first look at CMIP6 is also taken, but because the region with the strongest intermodel correlations is shifted towards Antarctica, further investigation is warranted in a separate study. After outlining the data and methods (Section 2), the relationships between baseline absolute temperature and a range of other climate variables, for both baseline and future changes, are examined (Section 3). Finally, the conclusions of this study are summarized in Section 4.

1.1. Data and Methods

This study focusses on CMIP5 models, but some preliminary analysis is conducted on available CMIP6 output. For CMIP5, the *historical* experiments are analyzed together with the Representative Concentration Pathway 8.5 (RCP8.5) scenario experiments (*rcp85*), through to the end of the 21st Century. The *rcp85* scenario was chosen since it has the strongest forcing, and therefore the largest projected changes, which helps to draw out possible correlations.

Baseline temperature is the equilibrium temperature that models achieve after a 'spin-up' period. In this study, the baseline temperature is evaluated in the early part of the *historical* simulations, i.e., the late 19th Century. The baseline period is taken as 1861 – 1900, early in the *historical* simulations and soon after the pre-industrial state. Greenhouse gas forcing may cause some temperature change in this early period, but the *historical* simulations are analyzed in preference over the pre-industrial control (*piControl*) simulations, since *piControl* data are available from fewer models than *historical* data. For projected changes, a difference is taken over the future period 2061 – 2100 and the baseline. Long reference periods of 40 years were chosen to reduce the influence of internal decadal variability as much as possible.

The primary climate variables analyzed here are surface air temperature (CMIP variable name: *tas*), TOA outgoing shortwave radiation (*rsut*), total cloud fraction (*clt*), surface zonal wind stress (*tauu*), and sea ice concentration (*sic*). All available CMIP5 monthly data for each of the five variables were gathered from both *historical* and *rcp85* experiment sets. Annual means were computed, and then the data were regridded to a common $1° \times 1°$ global grid. For models with multiple ensemble members, a single model ensemble mean was taken. Utilizing only models for which all five variables were available over the period 1861 – 2100 (after appending *rcp85* to *historical*), resulted in a set of 40 CMIP5 models (Table 1).

Net TOA radiation is also analyzed in the 40 CMIP5 models, but only in the *historical* experiments. It is computed as TOA incident shortwave radiation (*rsdt*) minus TOA *rsut* minus TOA outgoing longwave (*rlut*). Some relationships with ECS are computed, which is only available for 30 of these CMIP5 models (Table 1).

Surface air temperature is analyzed later in a group of CMIP6 models, using *historical* data together with *ssp585* (Table 2). Note that CMIP6 uses updated historical forcings, and the Shared Socioeconomic Pathway 5–8.5 (SSP5-8.5) is not identical to RCP8.5 in CMIP5 (O'Neill et al., 2016), but the differences are not expected to have appreciable impact on the analyses presented here.

TOA outgoing shortwave radiation is effectively a proxy for TOA albedo, and it is analyzed here in preference to net radiation to avoid conflation with other atmospheric and surface processes. The surface zonal wind stress is used to estimate the mean latitude of the eddy-driven jet. After regridding zonal wind stress to the common $1° \times 1°$ global grid, zonal means were taken. The jet latitude was then computed by fitting a quadratic polynomial to the latitude and two neighboring grid latitudes where zonal wind stress is maximal in the Southern Hemisphere. This method is similar to that of Kidston & Gerber (2010), but they use 10 m zonal wind data rather than zonal wind stress, which results in similar eddy-driven jet latitudes.

Regression coefficients are calculated using ordinary least squares, and quoted correlation values are Pearson's correlation coefficients. "Intermodel correlations" or regressions refer to the relationship between two variables across the models. For example, the intermodel correlation between absolute baseline GMST and GMST change is simply the correlation between absolute baseline GMST (from each of the 40 CMIP5 models) and GMST change (in the same 40 models). The symbol r is used to denote intermodel correlation. The 95% and 99% statistical confidence levels of correlations are quoted in various cases, which are tested using a Student's t-distribution. For a sample size of 40, correlations with magnitude greater than ~0.31 are significant at the 95% level ($p = 0.05$), and ~0.40 at the 99% level ($p = 0.01$).

In comparisons with reanalysis, the NOAA-CIRES-DOE Twentieth Century Reanalysis, version 3 (20CRv3) product is utilized (Compo et al., 2011). All five variables are from the "Monolevel" set (https://psl.noaa.gov/data/gridded/data.20thC_ReanV3.monolevel.html), using the monthly mean and ensemble mean data. GMST is computed from 2 m air temperature (variable name: *air.2m*), and the jet latitude from surface u-component momentum flux (*uflx*) following the same procedure as for the CMIP5 models. Other variables used are surface ice concentration (*icec*), upward shortwave radiation flux nominal at top-of-atmosphere (*uswrf.ntat*), and total cloud cover with entire atmosphere considered as a single layer (*tcdc.eatm*).

Table 1
List of Coupled Model Intercomparison Project, Phase 5 Models and Ensemble Members Analyzed in This Study.

	Model name	Ensemble members used	Exceptions	ECS (°C)
1	ACCESS1-0	r1i1p1		3.83
2	ACCESS1-3	r1i1p1		3.54
3	bcc-csm1-1	r1i1p1		2.83
4	bcc-csm1-1-m	r1i1p1		2.91
5	BNU-ESM	r1i1p1		4.04
6	CanESM2	r1i1p1, r2i1p1, r3i1p1, r4i1p1, r5i1p1		3.71
7	CCSM4	r1i1p1, r2i1p1, r3i1p1, r4i1p1, r5i1p1, r6i1p1	Missing for *clt*: r6i1p1	2.95
8	CESM1-BGC	r1i1p1		2.89[a]
9	CESM1-CAM5	r1i1p1, r2i1p1, r3i1p1	Missing for *clt*: r1i1p1, r2i1p1	4.10[b]
10	CMCC-CESM	r1i1p1		
11	CMCC-CM	r1i1p1		
12	CMCC-CMS	r1i1p1		
13	CNRM-CM5	r1i1p1, r2i1p1, r4i1p1, r6i1p1, r10i1p1		3.25
14	CSIRO-Mk3-6-0	r1i1p1, r2i1p1, r3i1p1, r4i1p1, r5i1p1, r6i1p1, r7i1p1, r8i1p1, r9i1p1, r10i1p1		4.06
15	FGOALS-g2	r1i1p1		3.35
16	FGOALS-s2	r1i1p1, r2i1p1, r3i1p1	Missing for *rsut* and *clt*: r1i1p1	4.19
17	FIO-ESM	r1i1p1, r2i1p1, r3i1p1		
18	GFDL-CM3	r1i1p1		4.00
19	GFDL-ESM2G	r1i1p1		2.43
20	GFDL-ESM2M	r1i1p1		2.45
21	GISS-E2-H	r1i1p1, r1i1p2, r1i1p3, r2i1p1, r2i1p3	Missing for *tauu*: r2i1p1, r2i1p3	2.30
22	GISS-E2-H-CC	r1i1p1		
23	GISS-E2-R	r1i1p1, r1i1p2, r1i1p3, r2i1p1, r2i1p3	Missing for *tas*: r1i1p3Missing for *tauu*: r2i1p1, r2i1p3	2.11
24	GISS-E2-R-CC	r1i1p1		
25	HadGEM2-AO	r1i1p1, r2i1p1, r3i1p1	Missing for *clt*: r2i1p1, r3i1p1	
26	HadGEM2-CC	r1i1p1		
27	HadGEM2-ES	r1i1p1, r2i1p1, r3i1p1, r4i1p1		4.58
28	inmcm4	r1i1p1		2.08
29	IPSL-CM5A-LR	r1i1p1, r2i1p1, r3i1p1, r4i1p1		4.13
30	IPSL-CM5A-MR	r1i1p1		4.14
31	IPSL-CM5B-LR	r1i1p1		2.60
32	MIROC-ESM-CHEM	r1i1p1		
33	MIROC-ESM	r1i1p1		4.66
34	MIROC5	r1i1p1, r2i1p1, r3i1p1		2.71
35	MPI-ESM-LR	r1i1p1, r2i1p1, r3i1p1		3.63
36	MPI-ESM-MR	r1i1p1		3.45
37	MRI-CGCM3	r1i1p1		2.61
38	MRI-ESM1	r1i1p1		

Table 1
Continued

	Model name	Ensemble members used	Exceptions	ECS (°C)
39	NorESM1-M	r1i1p1		2.82
40	NorESM1-ME	r1i1p1		2.99[c]

Ensemble members from the *historical* experiments were matched with ensemble members with the same identifiers from the *rcp85* experiments. The five primary variables analyzed in this study (*tas*, *rsut*, *clt*, *tauu*, and *sic*) were available from all models and ensemble members, unless noted under "exceptions". The equilibrium climate sensitivity (ECS) is recorded for models where available, and taken from Caldwell et al. (2016; their Table 1 and Equation 2), with three exceptions: [a]Nohara et al. (2015), [b]Meehl et al. (2013), [c]Seland et al. (2020)

2. Results

2.1. Baseline Temperature and Climate Sensitivity

Across CMIP5 models, the GMST in the baseline period (1861–1900) spans a range of 2.8°C (12.1°C – 14.9°C; Figure 1a). Following the evolution of global temperature through the historical simulations, and extending with the RCP8.5 emissions scenario, the projected range in absolute temperature is 3.9°C (15.5°C – 19.4°C in the future period 2061–2100; Figure 1a). By considering GMST anomalies with respect to the baseline period in each model, the projected range across all models is 2.5°C (2.9°C – 5.3°C), largely in agreement with Collins et al. (2013). The range of simulated absolute baseline temperatures therefore represents a considerable source of uncertainty in future projections.

There is no significant correlation between the absolute baseline GMST and GMST change across CMIP5 models under the RCP8.5 scenario (Figure 1b), consistent with earlier studies (Flato et al., 2013; Hawkins & Sutton, 2016). However, there is a striking feature in the spatial pattern of intermodel correlations between grid-point baseline surface temperature and GMST change (Figure 1c). Most of the Southern Ocean baseline temperature is negatively correlated with GMST change (with a grid-point maximum of $r = -0.64$). The intermodel correlation of the baseline temperature averaged over 35 – 55°S and GMST change is $r = -0.53$ (Figure 1d). Hence, models with initially cooler Southern Ocean surface temperature tend to warm more globally, vice versa for models with initially warmer Southern Ocean. Another notable feature in the spatial pattern is the north-south hemisphere contrast (Figure 1c), which appears somewhat analogous with the projection of a faster warming of the Northern Hemisphere than the Southern Hemisphere (e.g., Xie et al., 2010). The intermodel correlation between north-south hemisphere temperature difference in the baseline and GMST change is statistically significant ($r = 0.55$; figure not shown). But subsequent analysis is focussed on the Southern Ocean baseline temperature, since that is where the intermodel correlations are most prominent.

In contrast to Grise et al. (2015), here the intermodel relationship between baseline surface air temperature (as opposed to net TOA radiation) and global mean temperature change (as opposed to ECS; see their Figure 2a) is shown (Figure 1c). By analyzing surface air temperature change, rather than ECS, the model set is greatly expanded (output from 40 models here, cf. 20 models in Grise et al., 2015). Even though global mean temperature change is strongly related to ECS (Figure 2a) and baseline surface air temperature is strongly related to net TOA radiation (Figure 2b), the patterns shown in Figure 1c and by Grise et al. (2015; their Figure 2a for CMIP5) are substantially different. Some exploration reveals that selected baseline years (1861 – 1900 as opposed to 1990 – 1999, when anthropogenic forcings are stronger), the length of the baseline period (40 years as opposed to 10 years, which can be influenced by decadal variability), and the set of sampled models, all modify the pattern to some extent. However, exchanging only net TOA radiation with surface air temperature considerably strengthens the intermodel correlations over the Southern Ocean (cf. Figures 2c and 2d). Our subsequent focus is therefore on the Southern Ocean baseline surface temperature, and its relationship with key variables in the region, such as sea ice, cloud cover, and the westerly jet.

2.2. Links Between Surface Temperature and Baseline Climate

There are statistically significant intermodel regressions and correlations, but to differing levels, between the Southern Ocean baseline temperature and a range of other baseline climate variables in the domain,

Table 2
List of Coupled Model Intercomparison Project, Phase 6 Models and Ensemble Members Analyzed in This Study.

	Model name	Ensemble member used
1	ACCESS-CM2	r1i1p1f1
2	ACCESS-ESM1-5	r1i1p1f1
3	AWI-CM-1-1-MR	r1i1p1f1
4	BCC-CSM2-MR	r1i1p1f1
5	CAMS-CSM1-0	r1i1p1f1
6	CanESM5-CanOE	r1i1p2f1
7	CanESM5	r1i1p1f1
8	CESM2	r1i1p1f1
9	CESM2-WACCM	r1i1p1f1
10	CNRM-CM6-1	r1i1p1f2
11	CNRM-CM6-1-HR	r1i1p1f2
12	CNRM-ESM2-1	r1i1p1f2
13	EC-Earth3	r1i1p1f1
14	EC-Earth3-Veg	r1i1p1f1
15	FGOALS-f3-L	r1i1p1f1
16	FGOALS-g3	r1i1p1f1
17	FIO-ESM-2-0	r1i1p1f1
18	GFDL-CM4	r1i1p1f1
19	GFDL-ESM4	r1i1p1f1
20	HadGEM3-GC31-LL	r1i1p1f3
21	INM-CM4-8	r1i1p1f1
22	INM-CM5-0	r1i1p1f1
23	IPSL-CM6A-LR	r1i1p1f1
24	KACE-1-0-G	r1i1p1f1
25	MCM-UA-1-0	r1i1p1f2
26	MIROC6	r1i1p1f1
27	MIROC-ES2L	r1i1p1f2
28	MPI-ESM1-2-HR	r1i1p1f1
29	MPI-ESM1-2-LR	r1i1p1f1
30	MRI-ESM2-0	r1i1p1f1
31	NESM3	r1i1p1f1
32	NorESM2-LM	r1i1p1f1
33	UKESM1-0-LL	r1i1p1f2

Ensemble members from the *historical* experiments were matched with same identifiers from the *ssp585* experiments.

such as shortwave radiation, cloud cover, the meridional position of the westerly eddy-driven jet, and sea ice area (Figure 3). Here the spatial patterns are intermodel regressions (Figures 3a, 3c ,3e and 3g), rather than intermodel correlations (Figures 1 and 2).

Across all models, the baseline surface temperature area-averaged over 35 – 55°S is negatively related with TOA outgoing shortwave radiation in the Southern Ocean region (Figures 3a and 3b). TOA outgoing shortwave radiation is due mainly to albedo effects, and therefore the Southern Ocean baseline temperature is unsurprisingly also negatively related with cloud fraction (Figures 3c and 3d). Taken together, these results (Figures 3a–3d) show that models with warmer Southern Ocean surface temperatures tend to have less cloud cover and therefore less TOA outgoing shortwave radiation, and vice versa for models with cooler Southern Ocean surface temperature. The direct intermodel correlation between baseline Southern Ocean cloud cover and TOA outgoing shortwave radiation is particularly strong ($r = 0.75$; Figure 4).

The intermodel relationship of warmer Southern Ocean surface temperature and less cloud cover may seem counterintuitive, but the tendency for higher temperatures leading to increased cloudiness is more typical in the tropics. Higher temperatures throughout the tropical atmospheric column leads to greater cloud water content, due to an increased moist adiabatic lapse rate (Betts & Harshvardhan, 1987; Frey et al., 2018). On the other hand, cooler surface temperatures in the midlatitudes promote subsidence and the formation of reflective low-level clouds (Grise & Medeiros, 2016; Klein & Hartmann, 1993), and low clouds over the Southern Ocean exhibit the strongest sensitivity to surface temperature (Wall et al., 2017). In CMIP5, Southern Ocean sea surface temperature biases have been linked to cloud-related shortwave errors (Hyder et al., 2018). Therefore, the striking negative intermodel regression over the Southern Ocean band (Figure 3c) is likely due to models with less cloud cover permitting a greater downward shortwave radiation flux to heat the ocean surface.

The latitude of the Southern Hemisphere eddy-driven jet is also related to Southern Ocean surface temperature across models (Figures 3e and 3f). It has previously been shown that the jet latitude is biased equatorward in all CMIP3 models (Kidston & Gerber, 2010), and there is little improvement in CMIP5 (Barnes & Polvani, 2013). The jet latitude biases have been linked to shortwave cloud forcing biases (Ceppi et al., 2012). In models with cooler Southern Ocean surface temperature, the jet is more equatorward, and vice versa for models with warmer Southern Ocean ($r = -0.55$; Figure 3f). In atmosphere-only (AMIP) simulations of CMIP5, the mean model bias in jet latitude was found to be only 28% smaller, implying that surface temperature is only partly responsible, with most of the bias due to atmospheric processes (Bracegirdle et al., 2013). Kidston et al. (2011) found a seasonal link between jet latitude and sea ice area, but only during the cold season. Here, the direct relationship between baseline sea ice area and jet latitude is found to be weak ($r = -0.18$; Figure 4). Since the storm tracks are embedded in the eddy-driven jet, it is not surprising to find a positive intermodel correlation with cloudiness ($r = 0.38$; Figure 4) and therefore also with TOA outgoing shortwave radiation, due to albedo effects ($r = 0.67$; Figure 4).

There is a statistically significant relationship between baseline Southern Ocean temperature and Antarctic sea ice area ($r = -0.36$; Figure 3h), with stronger regression relationships near the edge of the sea ice region (Figure 3g). This is due to the strong link between local surface temperature and the presence of sea ice:

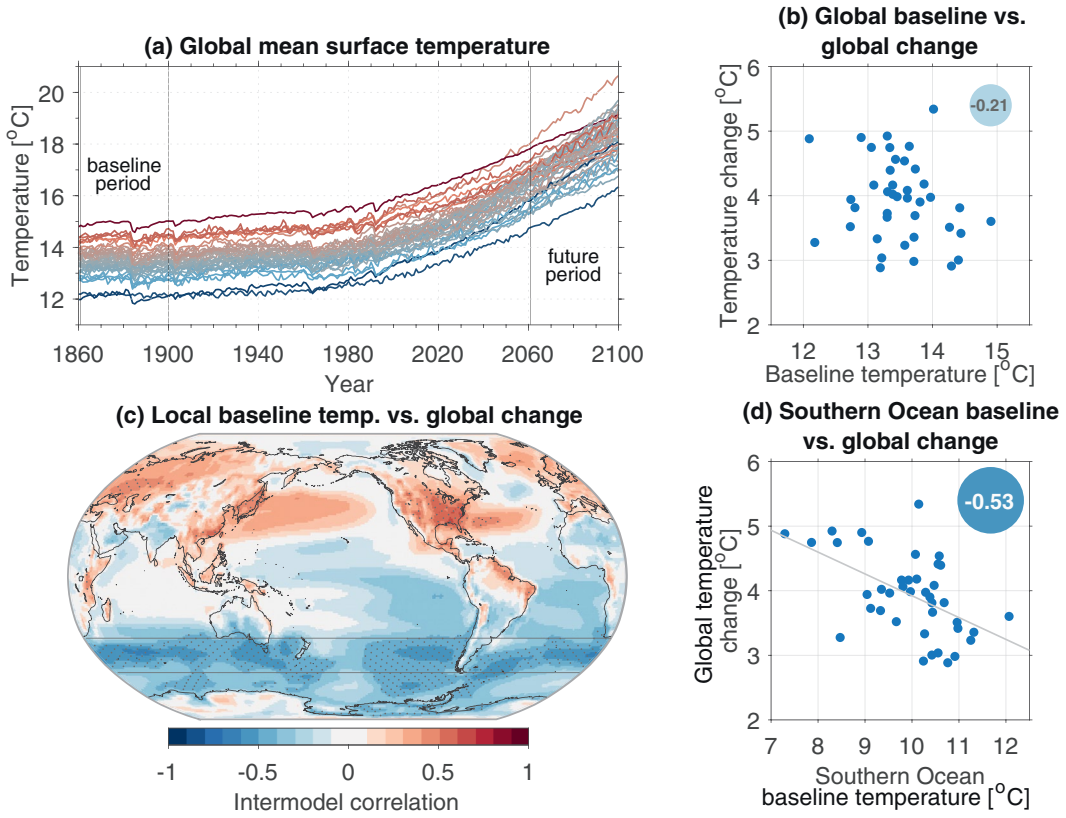

Figure 1. Intermodel surface air temperature relationships across Coupled Model Intercomparison Project, phase 5 (CMIP5). (a) Absolute annual global mean surface temperature (GMST) in CMIP5 historical simulations with representative concentration pathway 8.5 (RCP8.5) extension. The baseline (1861 – 1900) and future (2061 – 2100) periods are indicated. The timeseries are qualitatively shaded by baseline GMST: initially cooler models in blue and warmer models in red. (b) GMST averaged over the baseline period, versus the GMST change (i.e., average over future period minus average over baseline). The intermodel correlation ($r = -0.21$) is quoted, but $p > 0.05$. (c) Intermodel correlation between grid-point (local) baseline surface air temperature, from each of the 40 models, and GMST change, again from each of the 40 models. Stippling indicates where correlations are statistically significant at the 99% level. The Southern Ocean region (35–55°S) analyzed throughout this study is indicated. (d) Baseline surface air temperature averaged over the Southern Ocean, versus the GMST change. The intermodel correlation ($r = -0.53$) is statistically significant at $p < 0.01$.

surface temperature is substantially lower when sea ice is present, as opposed to when it is warmed by the open ocean below. In a positive feedback, cooler temperature also permits sea ice expansion. Conversely, higher temperature inhibits sea ice formation, and less sea ice exposes more water to solar radiation. Furthermore, the relatively cooler Antarctic waters are transported northward via Ekman advection. The feedback is illustrated to some extent in composite patterns of the 10 models with warmest and coolest baseline Southern Ocean surface temperature (Figure 5). There are strong temperature anomalies with respect to the model mean over the Antarctic sea ice region, in both baseline (Figures 5a and 5b) and projected temperature changes (Figures 5c and 5d). Thus, the intermodel relationship is physically consistent in that warmer models have less sea ice, and vice versa. Sea ice area correlates poorly with other variables across CMIP5, although there is a weak but statistically significant relationship with Southern Ocean cloud cover ($r = -0.35$; Figure 4), which may be related to sea ice suppression of evaporation (Bromwich et al., 2012).

2.3. Baseline Temperature and Future Projections

Thus far it has been shown that there are a range of physically consistent intermodel relationships between the baseline Southern Ocean surface temperature and a range of other baseline climate variables. But how are these relationships relevant to climate sensitivity? The relationships between baseline temperature and

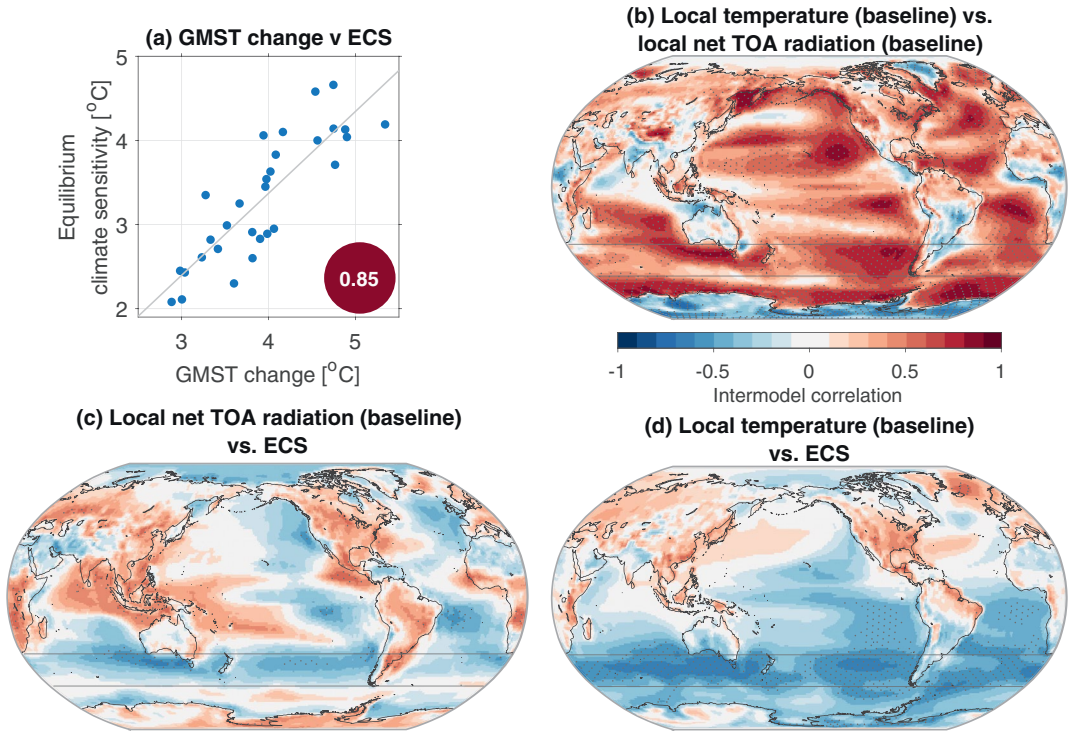

Figure 2. CMIP5 intermodel relationships between equilibrium climate sensitivity (ECS) and other variables. (a) Global mean surface air temperature (GMST) change versus ECS, for the 30 models for which the ECS value is available (Table 1). The intermodel correlation ($r = 0.85$) is statistically significant at $p < 0.01$. (b) Intermodel correlation between grid-point (local) baseline surface air temperature and grid-point baseline net top-of-atmosphere (TOA) radiation, across all 40 models. (c) Intermodel correlation between grid-point (local) net TOA radiation and ECS (30 models). (d) Intermodel correlation between grid-point (local) baseline surface air temperature and ECS (30 models). Stippling in each panel denotes statistically significant correlations at $p < 0.01$.

projected changes in variables are now examined. Changes in variables are computed under the RCP8.5 scenario, as a difference between the future (2061 – 2100) and baseline (1861 – 1900) periods (Figure 1a). A strong Southern Ocean signature also emerges in all of the spatial patterns of intermodel regressions (Figure 6), but here the relationships are positive.

The projected change in TOA outgoing shortwave radiation over the Southern Ocean is not consistent across models. In most models, outgoing radiation decreases into the future, but in a small number it increases (Figure 6b). Nevertheless, there is a statistically significant relationship between Southern Ocean temperature and the change in TOA outgoing shortwave radiation, such that there is a greater reduction in radiation (i.e., increased downward heat flux) for initially cooler models ($r = 0.49$; Figure 6b). Similarly, initially cooler models tend to lose more cloud cover under global warming ($r = 0.50$; Figure 6d). The similarities of the patterns in Figures 6a and 6c again reflect the strong link between outgoing shortwave radiation and cloud cover. The relationships with baseline temperature (Figures 6b and 6d) emerge despite the fact that there is no statistically significant relationship between the baseline and change in radiation ($r = -0.29$; Figure 4), nor between the baseline and change in cloud cover ($r = -0.25$; Figure 4). In other words, the baseline Southern Ocean temperature is a stronger predictor of changes in outgoing radiation and cloud cover than the baseline in each of these variables.

The eddy-driven jet is projected to shift poleward under all scenarios of climate change (Arblaster & Meehl, 2006; Miller et al., 2006; Simpson & Polvani, 2016). Furthermore, the future change in jet latitude appears to be closely connected to its baseline latitude, as was seen in CMIP3 models (Kidston & Gerber, 2010), and previously reported for CMIP5 (Simpson & Polvani, 2016). The more equatorward the jet is situated initially, the more poleward it shifts under global warming ($r = -0.62$; Figure 4). Since this correlation is between a variable and its change, the change contains a component of the baseline (i.e., A vs. B–A), and it is therefore

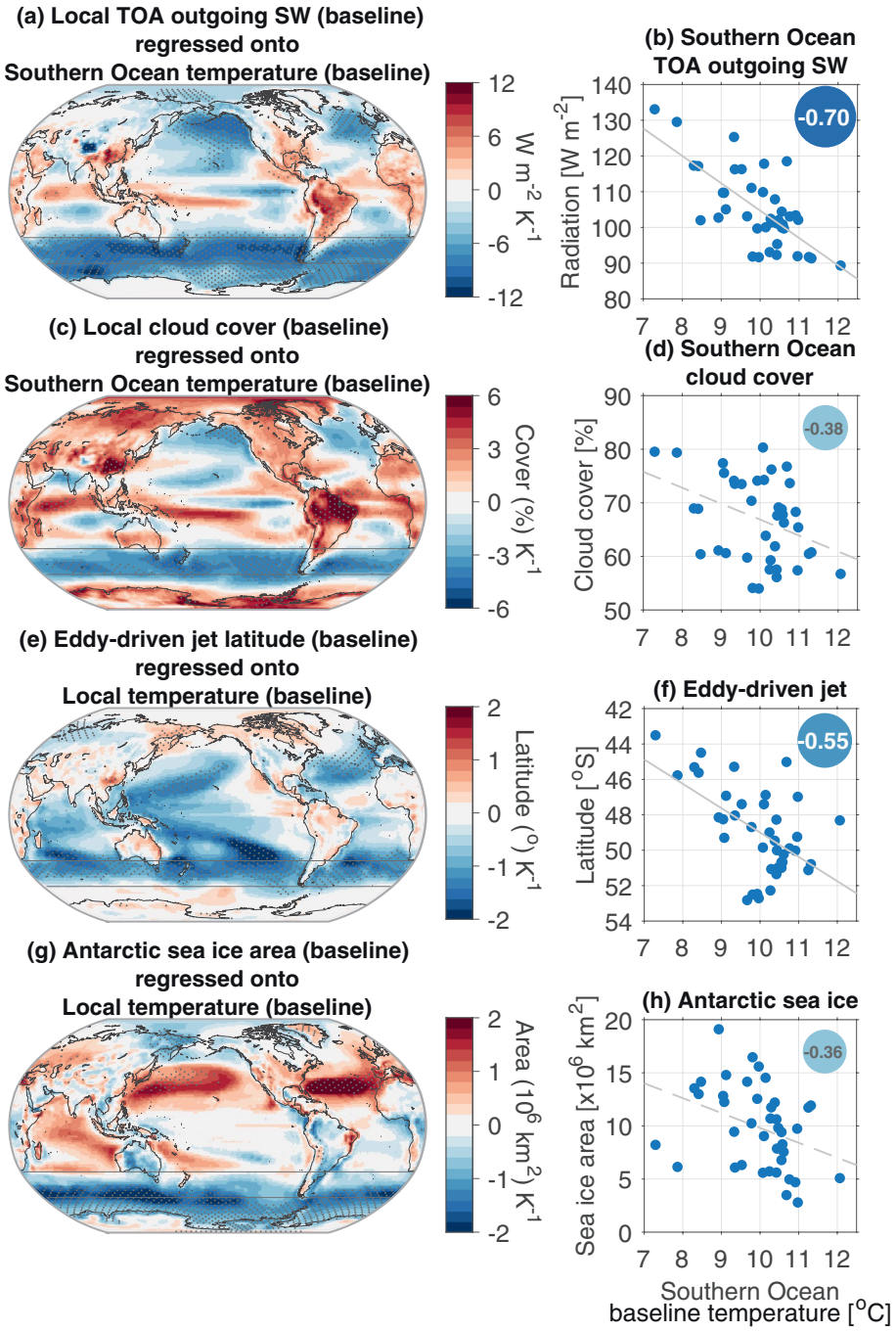

Figure 3. CMIP5 intermodel relationships between baseline surface temperature and other baseline variables. Intermodel regressions are shown in the left panels. In some cases, a field variable is regressed onto an index (a), (c), and in others an index is regressed onto a field (e), (g), but always onto baseline temperature, and expressed per unit Kelvin. In the panel titles, "local" denotes the field variable. (a) Top-of-atmosphere (TOA) outgoing shortwave radiation (field) regressed onto Southern Ocean temperature averaged over 35–55°S (index). (c) Cloud cover (field) regressed onto Southern Ocean average temperature (index). (e) Eddy-driven jet latitude (index) regressed onto temperature (field). (g) Total Antarctic sea ice area (index) regressed onto temperature (field). Stippling denotes statistically significant regressions at $p < 0.01$. The right panels show Southern Ocean baseline surface temperature averaged over 35–55°S (abscissa) versus baseline (b) Southern Ocean TOA outgoing shortwave radiation averaged over 35–55°S; (d) Southern Ocean cloud cover averaged over 35–55°S; (f) Eddy-driven jet latitude; and (h) Total Antarctic sea ice area. Intermodel correlations are quoted in the top right. Solid lines of best fit denote $p < 0.01$, and dashed lines denote $0.01 < p < 0.05$.

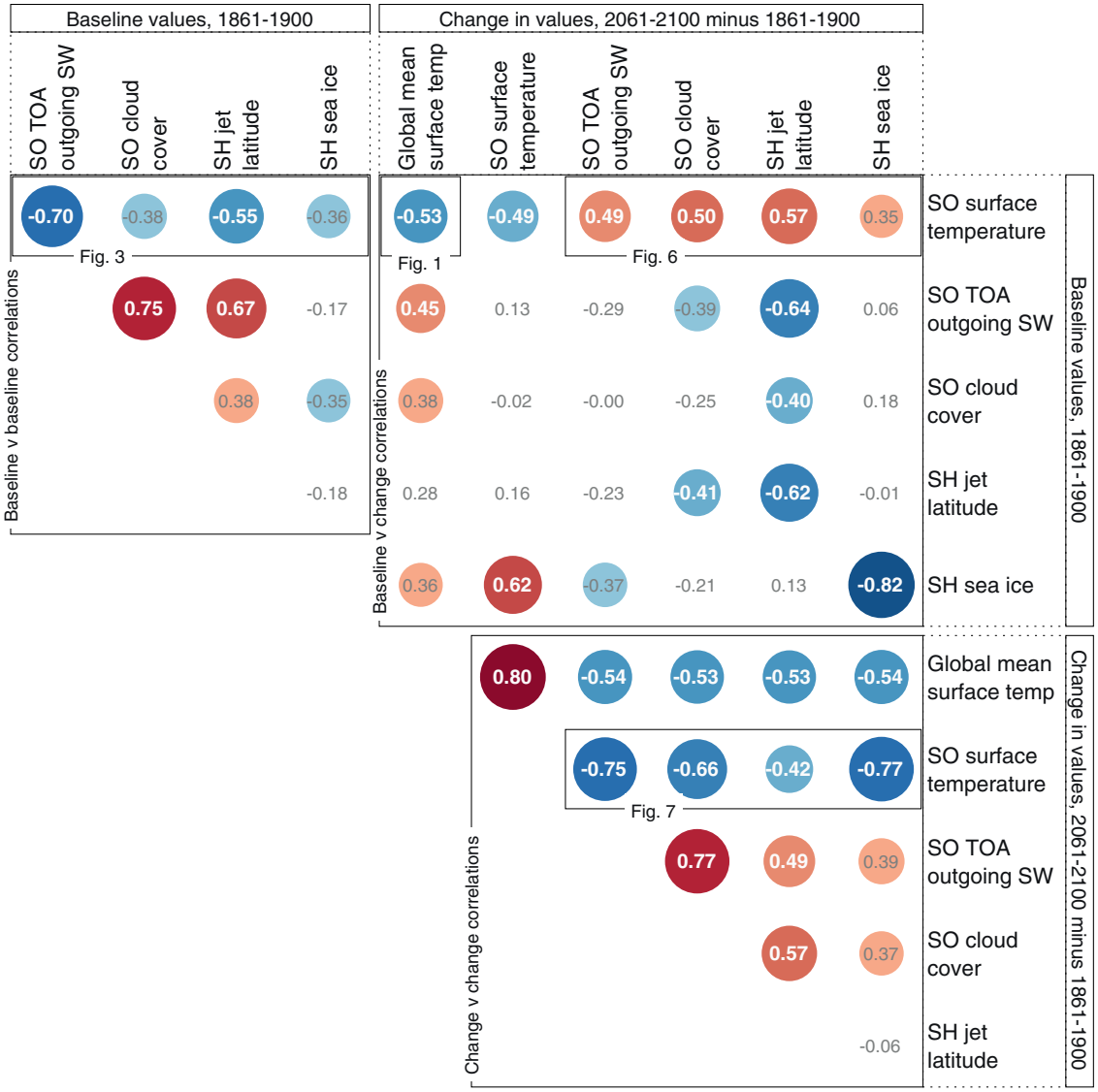

Figure 4. CMIP5 intermodel correlations between baseline values and future change values of all variables analyzed in this study. Red or blue shaded circles denote positive or negative correlations, respectively, where darker shades and larger circles denote stronger correlations. Correlations that are statistically significant at the 99% level are quoted in white text, and shaded circles are shown only where the correlations are statistically significant at the 95% level. The correlations shown in Figures 1, 3, 6 and 7 are indicated.

necessary to verify if the intermodel correlation is significant between the baseline latitude and the future latitude (i.e., A vs. B). In this case, the relationship is robust ($r = 0.92$; figure not shown).

The Southern Ocean baseline temperature is also a robust predictor of future jet migration, with initially cooler models exhibiting a larger shift in jet latitude ($r = 0.57$; Figure 6f). But unlike the Southern Ocean baseline temperature (Figure 1d), the baseline jet latitude position is not found to be a predictor for global mean surface temperature change ($r = 0.28$; Figure 4). Bracegirdle et al. (2018) found that baseline sea ice is more closely related to changes in jet strength, rather than latitude, where CMIP5 models with greater historical sea ice area exhibit less jet strengthening in the future. They likewise find that links between sea ice and jet shift are weak (here $r = 0.13$; Figure 4), albeit with some apparent seasonal relationships.

The intermodel regression of sea ice area change onto Southern Ocean baseline temperature (Figure 6g) has a similar pattern to baseline sea ice area regression (Figure 3g), also showing that local surface temperature nearer to the sea ice region is more closely related. But it is clear that models with initially more sea ice,

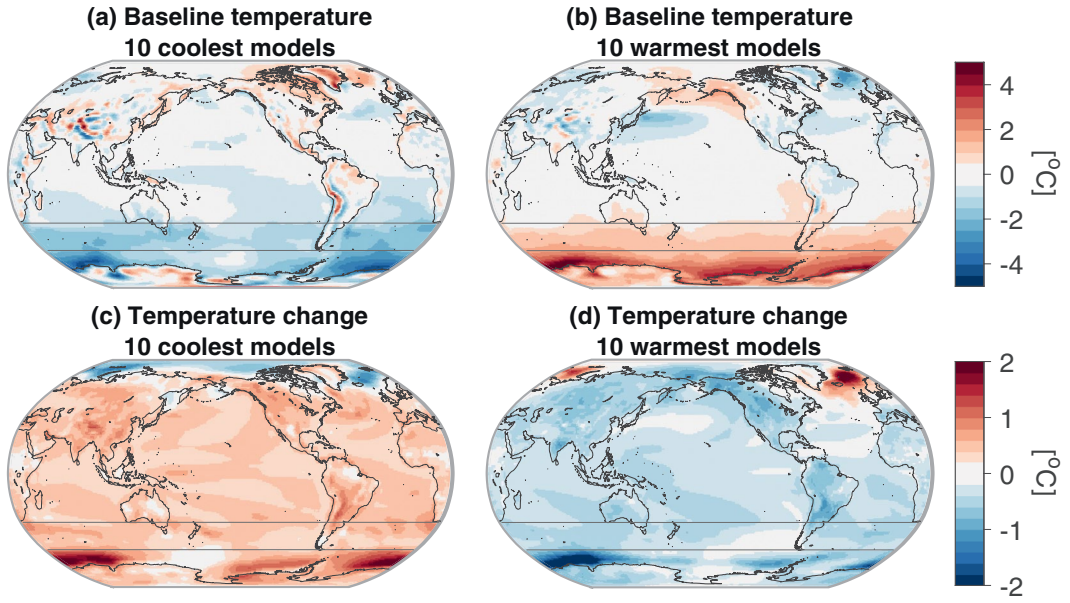

Figure 5. Composites of surface temperature in CMIP5 models by those with coolest and warmest baseline Southern Ocean surface temperature. (a) Mean baseline surface temperature in the 10 models with coolest Southern Ocean baseline temperature, shown as anomalies with respect to the model mean of all 40 models. (b) As in (a), but for the 10 warmest models. (c) Mean temperature change in the 10 models with coolest Southern Ocean baseline temperature, shown as anomalies with respect to the model mean of all 40 models. (d) As in (c), but for the 10 warmest models.

which correspond with models having cooler baseline Southern Ocean, also lose more sea ice under global warming ($r = -0.82$; Figure 4). As with the test for jet latitude, the direct intermodel correlation between baseline and future sea ice is similarly robust ($r = 0.87$; figure not shown).

The correlations between baseline Southern Ocean temperature and other baseline variables were found to be negative (Figure 3), whereas they are positive between baseline temperature and projected changes in other variables (Figure 6). At first glance, these "baseline-baseline" and "baseline-change" relationships may appear to be contradictory. But apart from a small number of exceptions, the projected changes in almost all variables and models are negative trending quantities (Figures 6b, 6d, 6f and 6h), i.e., sea ice, cloud cover, and outgoing radiation all tend to reduce in the future, and the jet tends to shift poleward. Therefore, the baseline-change relationships can be viewed as exhibiting weaker projected change in the initially warm-biased models, and greater change in the initially cold-biased models. Since it has been found that models with an initially cooler Southern Ocean exhibit greater global warming, the overall negative "change-change" intermodel regressions and correlations (Figure 7) are consistent. Hence, models with greater Southern Ocean temperature change exhibit greater change in other variables (Figures 7b, 7d, 7f and 7h).

It is postulated that these relationships between Southern Ocean temperature and future changes may emerge due to a "capacity for change" constraint. For example, a model with more sea ice initially has more sea ice to lose as the planet warms. Conversely, if a model has very little sea ice initially, then there is little capacity to lose sea ice. This idea is supported by the intermodel correlation between baseline and projected changes in sea ice ($r = -0.82$; Figure 4). A similar constraint may apply for the eddy-driven jet, without assuming that the jet itself directly influences the global climate. A jet that is situated more poleward initially would have less capacity to shift further poleward, and conversely a jet situated more equatorward would have more capacity to shift poleward. Again, this is supported by the intermodel correlation between the baseline and projected change in jet latitude ($r = -0.62$; Figure 4). Whilst it might be reasonable to expect a similar relationship for cloud cover, the intermodel correlation between baseline and projected change in cloud cover is not statistically significant ($r = -0.25$; Figure 4).

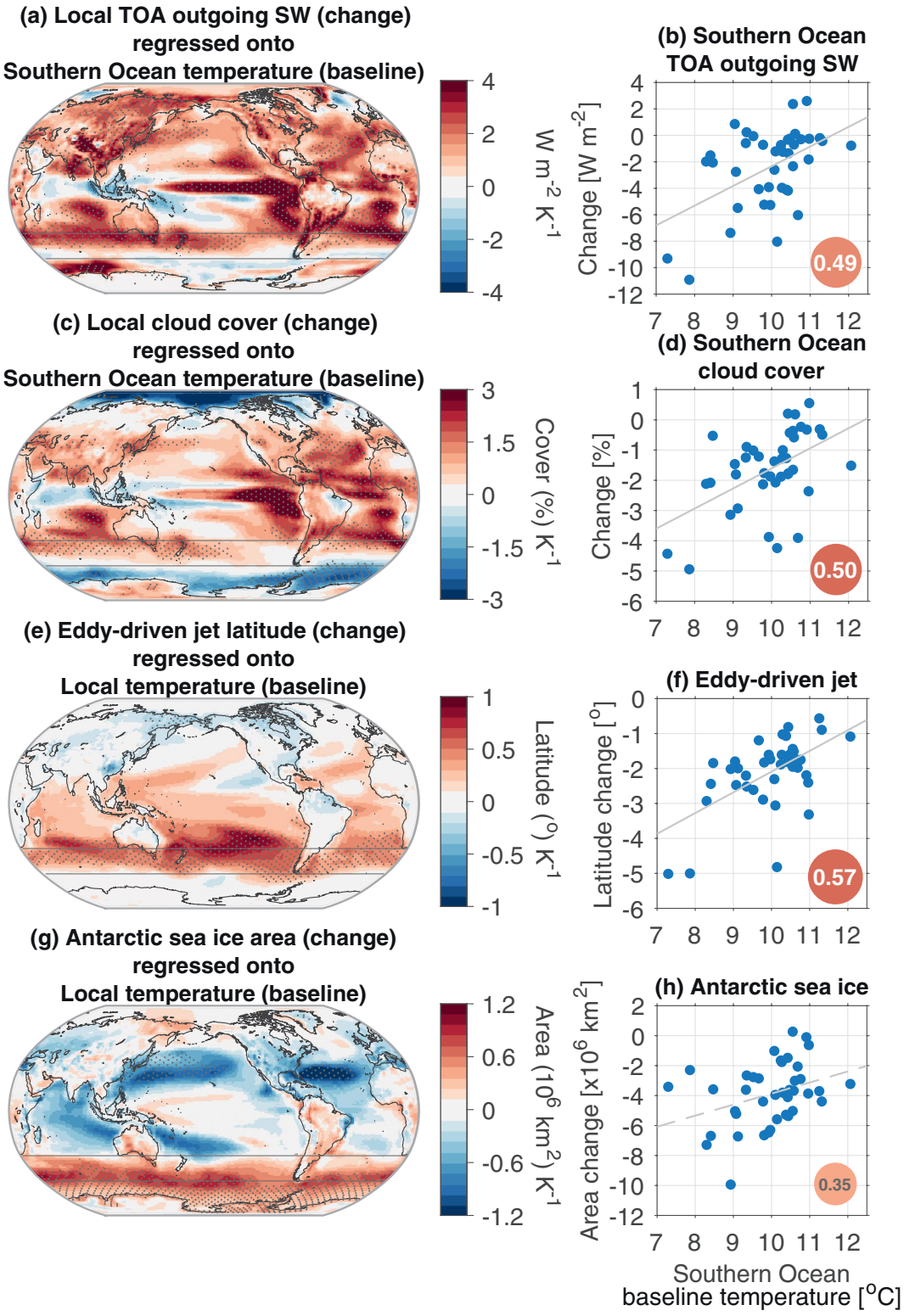
(a) Local TOA outgoing SW (change) regressed onto Southern Ocean temperature (baseline)
W m-2 K-1
(b) Southern Ocean TOA outgoing SW
Change [W m-2]
0.49
(c) Local cloud cover (change) regressed onto Southern Ocean temperature (baseline)
Cover (%) K-1
(d) Southern Ocean cloud cover
Change [%]
0.50
(e) Eddy-driven jet latitude (change) regressed onto Local temperature (baseline)
Latitude (°) K-1
(f) Eddy-driven jet
Latitude change [°]
0.57
(g) Antarctic sea ice area (change) regressed onto Local temperature (baseline)
Area (10^6 km^2) K-1
(h) Antarctic sea ice
Area change [x10^6 km^2]
0.35
Southern Ocean baseline temperature [°C]

Figure 6

Returning to the influence of surface temperature, future changes in all variables are not only correlated with Southern Ocean temperature changes (Figure 4; correlations in box marked "Figure 7"), but also with global mean temperature change (Figure 4; correlations above box marked "Figure 7"). Clearly, such correlations do not establish causation. However, the postulated capacity for change constraint provides some rationale as to how GMST change might be influenced by baseline Southern Ocean temperature amongst CMIP5 models.

2.4. Tests of Southern Ocean Emergent Constraints

The preceding analysis reveals that baseline Southern Ocean surface temperature in CMIP5 is a crucial variable in setting not only the baseline state of the Southern Ocean climate system, but also its future evolution and that of the global mean surface temperature (Figure 1). It is not necessarily possible to conclude that it is the single key variable, since most variables are coupled to one another. But it is nevertheless compelling that baseline temperature is the only variable that exhibits statistically significant correlations at the 95% level with all other baseline variables and their projected changes (Figure 4).

In an attempt to test the influence of baseline biases on GMST projections, the 40 CMIP5 models were subsampled according to whether they are biased above or below the NOAA 20th century reanalysis, for each of the variables (i.e., models to the left and right of reanalysis in Figure 8). In the first test, models were split into two groups according to whether their GMST is less than or greater than in the reanalysis, with both models and reanalysis averaged over 1961 – 2000. The period 1961 – 2000 was chosen since observations, and therefore reanalyses, are more uncertain in the earlier baseline period. The projected GMST change in the future period (2061 – 2100) minus the baseline period (1861 – 1900) was then examined in the two sets.

The mean GMST change in the warmer model set is less than the cooler model set, but there are only seven models in the warmer set (Figure 8a). A two sample Student's t-test for different means, but assuming unequal variance, reveals that the model-means of future warming in the two sets are not significantly different ($p = 0.33$). However, unsurprisingly, if the models are separated based on Southern Ocean surface temperature, then the two sets are different at the 95% confidence level. This is consistent with the intermodel correlation between baseline Southern Ocean surface temperature and GMST change (Figure 1d). The test on GMST changes was then repeated after subsampling models based on 1961 – 2000 mean values of each of the other variables shown in Figures 8c–8f. None of the differences in sets were statistically significant, indicating that only the baseline Southern Ocean temperature bias is a robust predictor of GMST change.

Another question that arises from the findings of this study is whether the model range in GMST projections can be constrained by observations, in essence by following the emergent constraints approach. To this end, we took the subset of models that are closest to the reanalysis, in a given variable, and tested whether the GMST projections in that subsample are different to the remaining, more-biased, models. The process of subsampling was conducted for each of the baseline variables examined in this study. The purpose of this exercise, in other words, is to test whether reducing the bias in any baseline variable may significantly alter the range in warming projections, or climate sensitivity.

As a first test, the 13 models (approximately one third) with GMST closest to that in the NOAA 20th century reanalysis over 1961 – 2000 were subsampled. The range in GMST change in the future period (2061 – 2100) minus the baseline period (1861 – 1900) in the model subset was then compared to that in the remaining 27 models. The 13 least biased models warm slightly less than the remaining 27 models. However, a two

Figure 6. CMIP5 intermodel relationships between baseline surface temperature and projected changes in other variables. Intermodel regressions are shown in the left panels. In some cases, a field variable is regressed onto an index (a), (c), and in others an index is regressed onto a field (e), (g), but always onto baseline temperature, and expressed per unit Kelvin. In the panel titles, "local" denotes the field variable. (a) Top-of-atmosphere (TOA) outgoing shortwave radiation change (field) regressed onto Southern Ocean temperature averaged over 35–55°S (index). (c) Cloud cover change (field) regressed onto Southern Ocean average temperature (index). (e) Eddy-driven jet latitude change (index) regressed onto temperature (field). (g) Total Antarctic sea ice area change (index) regressed onto temperature (field). Stippling denotes statistically significant regressions at $p < 0.01$. The right panels show Southern Ocean baseline surface temperature averaged over 35 – 55°S (abscissa) versus projected changes in (b) Southern Ocean TOA outgoing shortwave radiation averaged over 35 – 55°S; (d) Southern Ocean cloud cover averaged over 35 – 55°S; (f) Eddy-driven jet latitude; and (h) Total Antarctic sea ice area. Intermodel correlations are quoted in the top right. Solid lines of best fit denote $p < 0.01$, and dashed lines denote $0.01 < p < 0.05$.

10.1029/2020EF001873

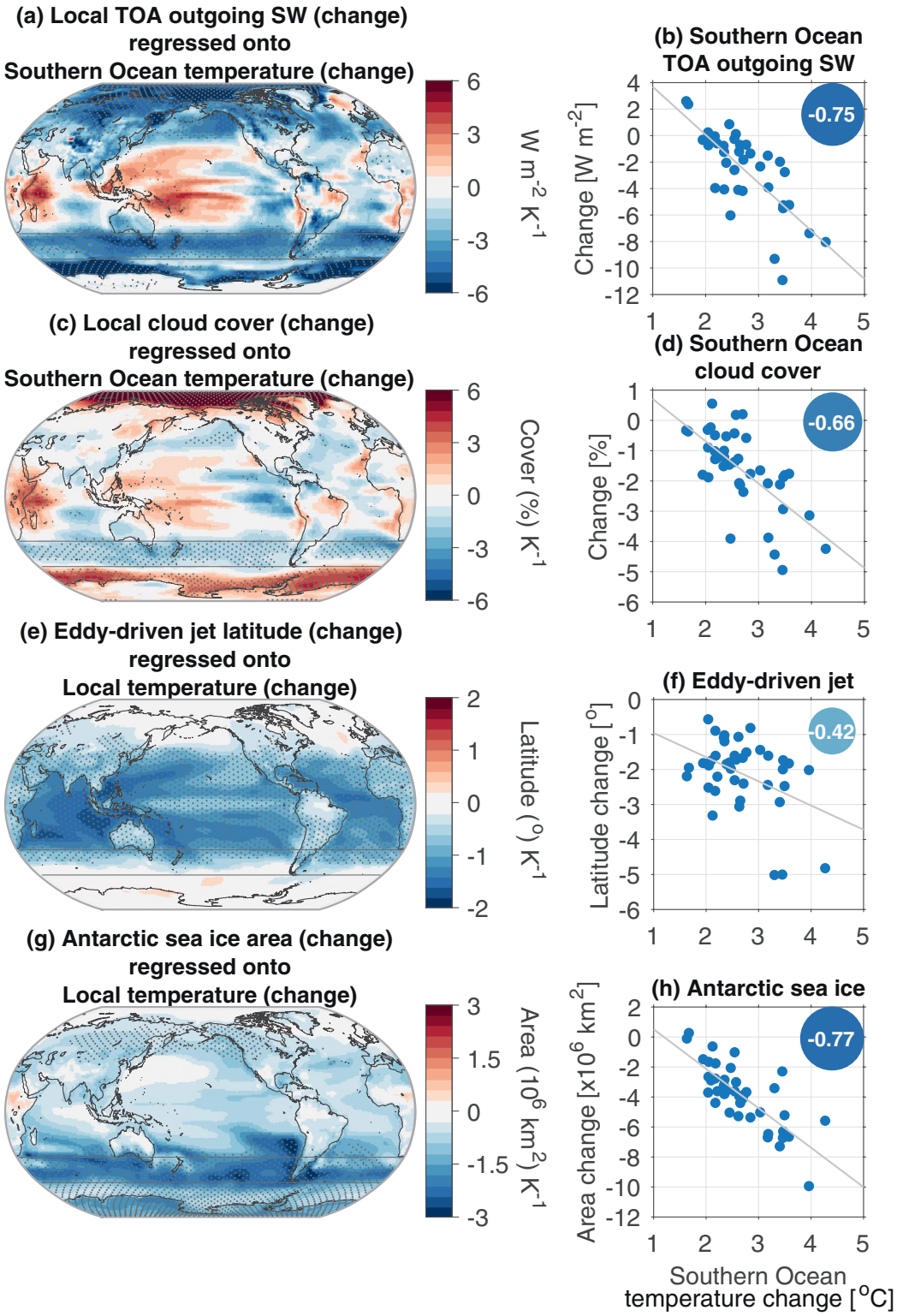

Figure 7

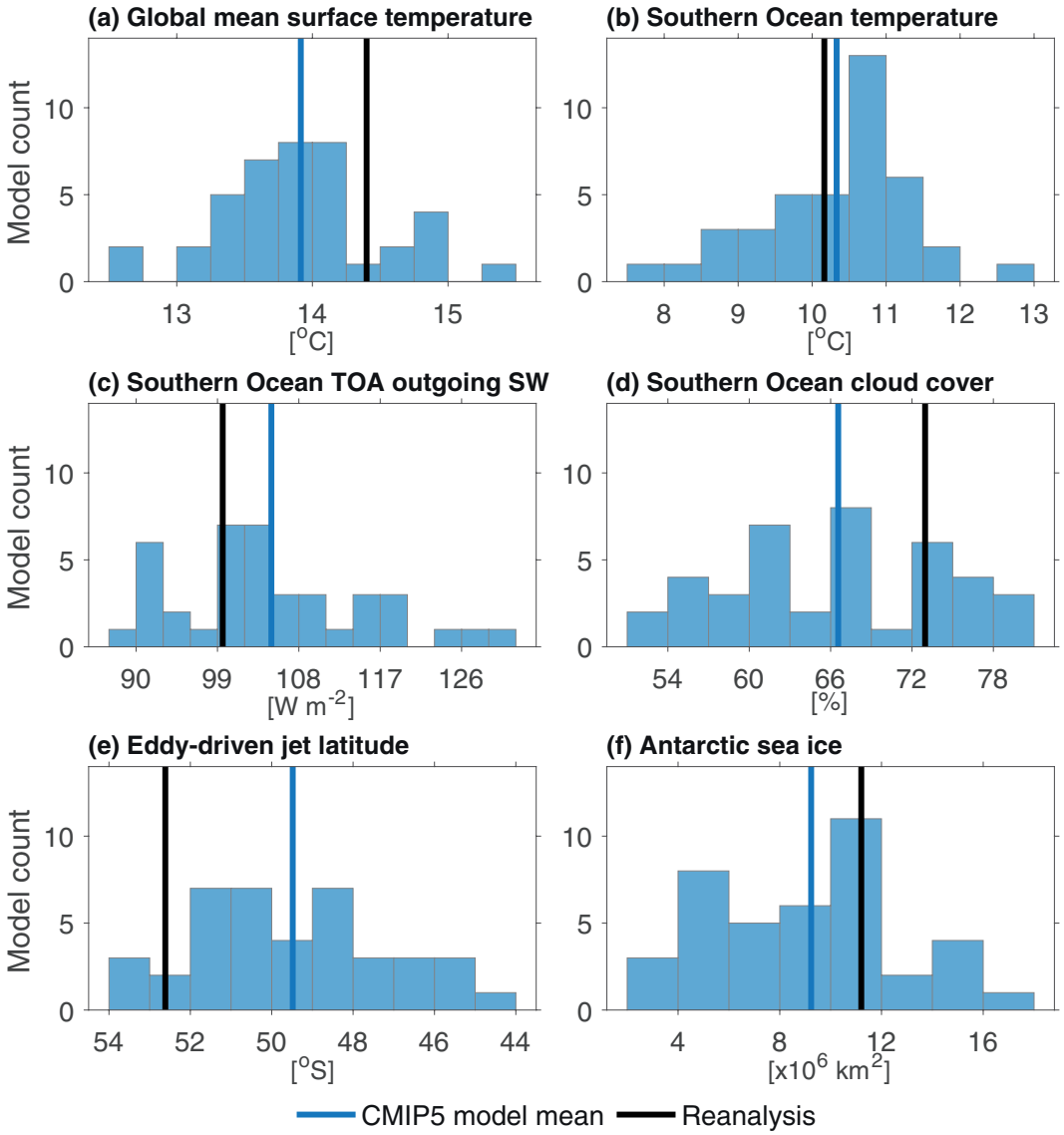

Figure 8. Histograms of variables in CMIP5 models, averaged over the period 1961 – 2000. The vertical blue line denotes the model mean, and the black line denotes the NOAA-CIRES-DOE Twentieth Century Reanalysis, version 3. (a) Global mean surface air temperature. (b) Surface air temperature averaged over the Southern Ocean. (c) Top-of-atmosphere outgoing shortwave radiation averaged over the Southern Ocean. (d) Cloud cover averaged over the Southern Ocean. (e) Eddy-driven jet latitude. (f) Antarctic sea ice area.

sample Student's *t*-test for different means, but assuming unequal variance, reveals that the model-means of future warming in the two sets are not significantly different ($p = 0.21$). Similarly, a two sample Kolomogorov-Smirnov test for the sets coming from different continuous distributions, or a two sample *F*-test

Figure 7. CMIP5 intermodel relationships between projected changes in surface temperature and projected changes in other variables. Intermodel regressions are shown in the left panels. In some cases, a field variable is regressed onto an index (a), (c), and in others an index is regressed onto a field (e), (g), but always onto temperature change, and expressed per unit Kelvin. In the panel titles, "local" denotes the field variable. (a) Top-of-atmosphere outgoing shortwave radiation change (field) regressed onto Southern Ocean temperature change averaged over 35 – 55°S (index). (c) Cloud cover change (field) regressed onto Southern Ocean average temperature change (index). (e) Eddy-driven jet latitude change (index) regressed onto temperature change (field). (g) Total Antarctic sea ice area change (index) regressed onto temperature change (field). Stippling denotes statistically significant regressions at $p < 0.01$. The right panels show change in Southern Ocean baseline surface temperature averaged over 35 – 55 S (abscissa) versus projected changes in (b) Southern Ocean TOA outgoing shortwave radiation averaged over 35 – 55 S; (d) Southern Ocean cloud cover averaged over 35 – 55°S; (f) Eddy-driven jet latitude; and (h) Total Antarctic sea ice area. Intermodel correlations are quoted in the top right. Solid lines of best fit denote $p < 0.01$, and dashed lines denote $0.01 < p < 0.05$.

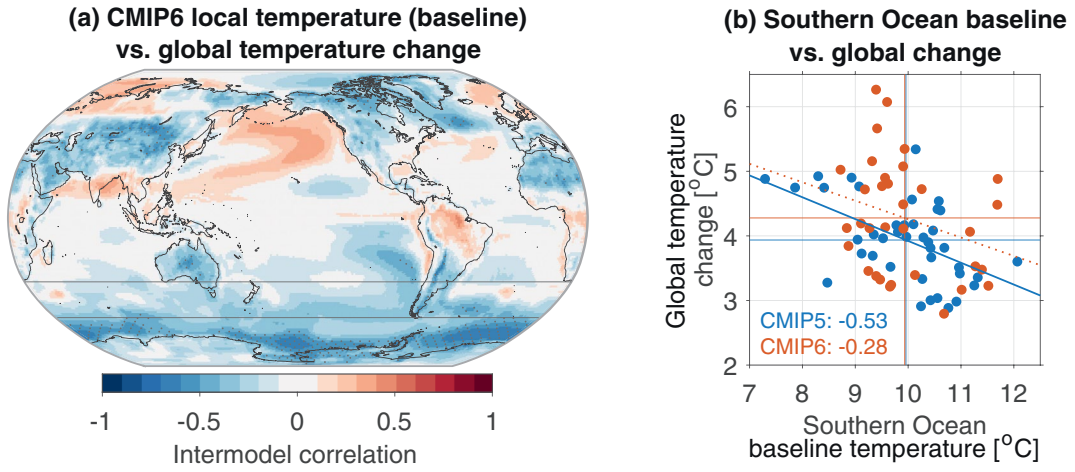

Figure 9. Coupled Model Intercomparison Project, phase 6 (CMIP6) intermodel relationships between baseline temperature and global mean surface temperature change. (a) Intermodel correlation in 33 CMIP6 models (Table 2) between grid-point (local) baseline surface air temperature and global mean surface air temperature change. Stippling indicates where correlations are statistically significant at the 99% level. CMIP6 surface air temperature is analyzed in the *historical* simulations with *ssp585* extension. (b) Baseline surface air temperature averaged over the Southern Ocean, versus the GMST change, in CMIP5 (blue; as in Figure 1c) and CMIP6 (red). The intermodel correlation coefficients for each model set are given at the bottom left of panel (b). The correlation is not statistically significant for CMIP6 ($p > 0.05$) and denoted by a dotted line. CMIP5 and CMIP6 multi-model means are denoted by vertical and horizontal lines in their respective colors.

for different variances, do not suggest that there are statistically significant differences in future projection distributions between the two sets.

The tests above were repeated after subsampling models based on 1961 – 2000 mean values of the other variables shown in Figures 8b–8f. For Southern Ocean TOA outgoing shortwave radiation, cloud cover, and Antarctic sea ice area, the 13 least biased models exhibit greater GMST change than in the remaining models. But for eddy-driven jet latitude and baseline Southern Ocean temperature, the 13 least biased models warm less. Subsampling based on eddy-driven jet latitude exhibits the largest differences between pairs of subsets. However, none of the pairs of subsets, for any variable, are significantly different under any of the aforementioned statistical tests. Altering the number of models in the subsample set made little difference. Based on these tests, efforts to constrain the model-mean and range of GMST projections, or climate sensitivity, by subsampling less biased models does not seem to be possible for CMIP5 models using these variables.

2.5. A First Look at Coupled Model Intercomparison Project, Phase 6

The following is a preliminary investigation of the surface temperature relationship in CMIP6. Although the correlations are mostly negative, the statistically significant intermodel correlation over the Southern Ocean seen in CMIP5 (Figure 1) is not present across the 33 models analyzed thus far in CMIP6 (Figure 9a). However, the region of statistically significant intermodel correlation is shifted to the south: the baseline surface temperature over most of the Antarctic sea ice region is negatively correlated with global mean surface temperature change. The Southern Ocean surface temperature range (Hyder et al., 2018) is slightly narrowed in CMIP6, with fewer models in the cold bias tail, but the multi-model means of the two sets are very similar (Figure 9b). A higher climate sensitivity in CMIP6 is apparent, with an increase in the multi-model mean of the GMST change, but the increase has been shown to be statistically insignificant (Zelinka et al., 2020).

The changing nature of intermodel relationships across model generations should not be too surprising. As key biases are tackled, and reduced or altered, different intermodel features may arise. For instance, as noted earlier, the strong CMIP3 intermodel relationship between Southern Hemisphere net TOA radiation and climate sensitivity (Trenberth & Fasullo, 2010) was substantially weaker across CMIP5 models (Grise

et al., 2015). Similarly, the CMIP5 Southern Ocean temperature relationship with GMST change is weaker in CMIP6, though the cause of this has not yet been revealed, and will be explored in a future study.

The analysis of CMIP6 is not taken further in this study for two reasons. Firstly, at the time of writing, the variables analyzed in CMIP5 were only sparsely available in CMIP6 across both historical and scenario runs. Over 130 models have registered their source identifiers for CMIP6 with the World Climate Research Programme, so many more simulations are expected to be available over the coming months and years. Secondly, the altered pattern in CMIP6 (cf. Figure 1c and Figure. 9) indicates that different processes or biases are at play. It is likely that CMIP6 analyses will reveal a different story altogether: one of the Antarctic region, rather than Southern Ocean dynamics. A new future study will focus on unraveling the processes underpinning this higher latitude link between baseline surface temperature biases and future warming.

Despite the current relatively small sample of CMIP6 models from the eventual number expected, some findings relevant to this study have emerged in the literature. It has been found, for example, that 10 out of 27 CMIP6 models analyzed simulate higher equilibrium climate sensitivity than any of those in CMIP5 (Zelinka et al., 2020). Although the shift in ECS range is statistically insignificant, the higher sensitivity in some models is due to a stronger reduction of lower level cloud cover under global warming, particularly in the Southern Hemisphere extratropics (Zelinka et al., 2020). Efforts to understand the plausibility of models with higher sensitivity is underway, with the recognition that substantially more CMIP6 simulations are expected. In terms of the global energy budget, CMIP6 is in better agreement with reference estimates than earlier model generations, and particularly for shortwave clear-sky budgets (Wild, 2020).

CMIP6 also appears to show a stronger intermodel relationship between the global temperature trends of the recent past (i.e., 1981–2014) and both equilibrium climate sensitivity and transient climate response, as compared with CMIP5 (Tokarska et al., 2020). This opens the potential for future warming estimates to be constrained by observations, as more CMIP6 models become available.

With regards to the other variables examined in this study, CMIP6 exhibits mixed results to date. Despite a larger under-representation in boreal summer Antarctic sea ice area in CMIP6 (Roach et al., 2020), there are nevertheless some positive signs of improvement. For example, there is a reduction in the intermodel spread of seasonal sea ice variations, and the regional distribution is improved, compared to CMIP5 (Roach et al., 2020). The Southern Hemisphere jet stream and storm tracks are also less biased in CMIP6, exhibiting higher mean jet latitude (Bracegirdle et al., 2020; Curtis et al., 2020; Goyal et al., 2021; Priestley et al., 2020), and therefore reduced jet shift under future warming (Curtis et al., 2020). The reduced jet stream bias is likely due to increased horizontal atmospheric resolution (Curtis et al., 2020). Along with improvements to the representation of surface wind stress forcing, the simulated strength of the Antarctic Circumpolar Current and associated density gradients have improved in CMIP6 (Beadling et al., 2020). The simulated mean sea level has also improved in the Southern Ocean (Lyu et al., 2020).

3. Discussion and Conclusions

A summary of the relationships revealed in this study is shown in Figure 10. The schematic illustrates overall CMIP5 model tendencies, for those with warmer or cooler Southern Ocean baseline temperature. The relationships for the baseline state are physically consistent, that is, with warmer Southern Ocean there is a tendency for less cloud, and therefore less TOA outgoing shortwave radiation, less sea ice and a more poleward eddy-driven jet (Figure 10a). Under global warming, in models with initially warmer Southern Ocean, there are lower reductions in sea ice, clouds, and TOA outgoing shortwave radiation, and smaller latitudinal shifts in the eddy-driven jet. Conversely, in models with initially cooler Southern Ocean, there is a tendency for initially larger cloud and sea ice area, higher TOA outgoing shortwave and an eddy-driven jet that is positioned more equatorward (Figure 10b). Under global warming, initially cooler models tend to simulate a greater poleward jet shift, and a greater reduction in outgoing shortwave, clouds, and sea ice cover. The schematic is an attempt to illustrate only overall model tendencies. The behaviors are not the same in each model, since not every model with an initially cool Southern Ocean, for instance, will involve all of the processes featured in Figure 10a. Furthermore, initial analysis indicates that this schematic will be somewhat different for CMIP6.

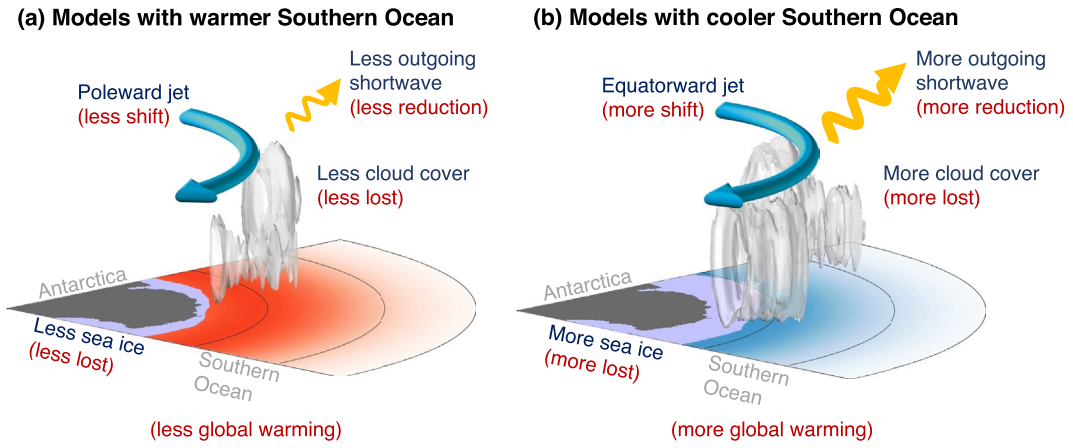

Figure 10. Schematic summary of model tendencies in CMIP5. (a) Models with warmer baseline Southern Ocean surface air temperature. (b) Models with cooler baseline Southern Ocean surface air temperature. Red text in parentheses indicate changes under global warming.

The upshot of these relationships in the Southern Ocean climate system is that models with an initially warmer Southern Ocean exhibit less global warming, and initially cooler models exhibit more global warming. It is postulated that this relationship between Southern Ocean baseline temperature and climate sensitivity in CMIP5 (Figure 1d) is due to a potential "capacity for change" mechanism. For example, cold-biased models tend to have more cloud cover, sea ice, and equatorward jet initially (Figures 3d, 3f and 3h), and thus a greater capacity to lose cloud cover and sea ice, or for the jet to shift poleward under global warming (Figures 6d, 6f and 6h). Reinforcing this postulation, it was found that greater projected changes in these variables correlated with not only greater Southern Ocean temperature change (Figures 7d, 7g and 7h), but also GMST change (Figure 4). Such intermodel correlations do not imply causation, but these findings may provide clues on where to focus future model development efforts.

Model developers have tended to approach the problem of Southern Ocean biases by using clouds as the controlling variable. Models generally do not simulate enough cloud cover over the Southern Ocean (Figure 8d), leading to too much incoming shortwave radiation at the surface, warm sea surface temperature biases, reduced sea ice, and a shift in the eddy-driven jet (Ceppi et al., 2012; Hyder et al., 2018; Williams et al., 2017). Since cloud schemes involve the fastest dynamical processes in the chain of causality, they are generally the aspect that model developers have found easiest to manipulate. An apparent consequence of modified cloud schemes has been an increase in climate sensitivities in many state-of-the-art models (Bodas-Salcedo et al., 2019; Zhu & Poulsen, 2020).

Model representations of clouds might be the key factor linking the Southern Ocean atmospheric processes together, and therefore influencing the simulation of the Southern Ocean baseline state. However, we found that the baseline cloud cover is not strongly linked to projected cloud cover change. In contrast, the baseline sea ice area and jet latitude both have strong intermodel correlations with their projected changes. Sea ice albedo has also been recognized as a key component of the global heat balance (Flato et al., 2013), and may be the source of an emergent constraint (Thackeray & Hall, 2019). The jet and sea ice extent can conspire to affect Southern Ocean baseline surface temperature via northward Ekman transport of Antarctic surface waters, in turn contributing to GMST change. The representation of clouds, however, would have a more direct impact on GMST via its global distribution. The findings of this study suggest that a more holistic investigation of the processes that contribute to setting the baseline temperature in models may be beneficial towards an understanding of the processes by which the baseline temperature influences regional and global climate changes.

Baseline absolute temperature was found to be a key variable in the Southern Ocean in CMIP5, since each of the other variables inspected exhibits a strong intermodel correlation with it, but not necessarily amongst themselves. However, we do not advocate that models be tuned for baseline temperature, if that even were plausible. In particular, all variables are coupled to one another: tuning a model for one particular baseline

variable would invariably alter the baseline states of other variables, and not necessarily yield a more realistic climate simulation. For instance, the intermodel correlations imply that an attempt to cool the Southern Ocean surface in a model which is initially too warm, might shift its jet latitude equatorward (Figure 3f), but it was shown that most models already have an equatorward bias in jet latitude (Figure 8e). There are similar inconsistencies when comparing with observations in other variables: For example, the model mean of Southern Ocean temperature is close to reanalysis (Figure 8b), and while cloud cover (Figure 8d) and sea ice (Figure 8f) are under-represented, there is a tendency for too much TOA outgoing shortwave radiation (Figure 8c). In a set of simple tests, we also found that it did not seem possible to constrain the spread in CMIP5 GMST projections by subsampling models that align more closely with reanalysis.

It was shown that in the first available CMIP6 models, the baseline temperature relationship with global mean temperature change is less pronounced over the Southern Ocean, which may be a result of model improvements. The position of the Southern Hemisphere mid-latitude jet, for instance, appears to be less biased (more poleward) across CMIP6 models. Instead, stronger intermodel correlations emerge in the Antarctic sea ice region, suggesting that biases in polar region dynamics in CMIP6, rather than mid-latitude Southern Ocean dynamics in CMIP5, might play a stronger role on global changes. As more CMIP6 model output becomes available, an examination of biases in the Antarctic region and their possible causal effect on GMST will be undertaken.

Data Availability Statement

Climate modeling groups produced and made their model output available (https://esgf-node.llnl.gov). CMIP5 and CMIP6 model outputs were made available with the assistance of resources from the National Computational Infrastructure (NCI), which is supported by the Australian Government. NOAA Physical Sciences Laboratory made the Twentieth Century Reanalysis data available (https://www.esrl.noaa.gov/psd/data/gridded/data.20thC_ReanV3.html).

Acknowledgments
This work was supported by the Natural Environment Research Council (SMURPHS project NE/N005783/1 and NE/N006348/1), and by the Australian Research Council Centre of Excellence for Climate Extremes (CE170100023). Agus Santoso and Matthew H. England are also supported by the Centre for Southern Hemisphere Oceans Research, a joint research center between QNLM and CSIRO, and by the Earth Systems and Climate Change Hub of the Australian Government's National Environmental Science Program. Andréa S. Taschetto is supported by the Australian Research Council (FT160100495). Leela M.Frankcombe is supported by the Australian Research Council (DE170100367). We acknowledge the World Climate Research Program (WCRP) Working Group on Coupled Modeling, which is responsible for the Coupled Model Intercomparison Project (CMIP). Support for the Twentieth Century Reanalysis Project version 3 data-set is provided by the U.S. Department of Energy, Office of Science Biological and Environmental Research (BER), by the National Oceanic and Atmospheric Administration Climate Program Office, and by the NOAA Physical Sciences Laboratory. The authors wish to thank the two anonymous reviewers for taking the time to review our manuscript. Their careful consideration and suggestions helped to substantially improve the presentation of this study.

References

Arblaster, J. M., & Meehl, G. A. (2006). Contributions of external forcings to southern annular mode trends. *Journal of Climate*, *19*(12), 2896–2905. https://doi.org/10.1175/JCLI3774.1

Barnes, E. A., & Polvani, L. M. (2013). Response of the midlatitude jets, and of their variability, to increased greenhouse gases in the CMIP5 models. *Journal of Climate*, *26*(18), 7117–7135. https://doi.org/10.1175/JCLI-D-12-00536.1

Beadling, R. L., Russell, J. L., Stouffer, R. J., Mazloff, M., Talley, L. D., Goodman, P. J., et al. (2020). Representation of Southern Ocean properties across Coupled Model Intercomparison Project generations: CMIP3 to CMIP6. *Journal of Climate*, *33*, 6555–6581. https://doi.org/10.1175/JCLI-D-19-0970.1

Betts, A. K., & Harshvardhan (1987). Thermodynamic constraint on the cloud liquid water feedback in climate models. *Journal of Geophysical Research*, *92*(D7), 8483–8485. https://doi.org/10.1029/jd092id07p08483

Bodas-Salcedo, A., Mulcahy, J. P., Andrews, T., Williams, K. D., Ringer, M. A., Field, P. R., & Elsaesser, G. S. (2019). Strong dependence of atmospheric feedbacks on mixed-phase microphysics and aerosol-cloud interactions in HadGEM3. *Journal of Advances in Modeling Earth Systems*, *11*, 1735–1758. https://doi.org/10.1029/2019MS001688

Bracegirdle, T. J., Holmes, C. R., Hosking, J. S., Marshall, G. J., Osman, M., Patterson, M., & Rackow, T. (2020). Improvements in circumpolar southern hemisphere extratropical atmospheric circulation in CMIP6 compared to CMIP5. *Earth and Space Science*, *7*, e2019EA001065. https://doi.org/10.1029/2019EA001065

Bracegirdle, T. J., Hyder, P., & Holmes, C. R. (2018). CMIP5 diversity in southern westerly jet projections related to historical sea ice area: Strong link to strengthening and weak link to shift. *Journal of Climate*, *31*, 195–211. https://doi.org/10.1175/JCLI-D-17-0320.1

Bracegirdle, T. J., Shuckburgh, E., Sallée, J. B., Wang, Z., Meijers, A. J. S., Bruneau, N., et al. (2013). Assessment of surface winds over the atlantic, indian, and pacific ocean sectors of the southern ocean in CMIP5 models: Historical bias, forcing response, and state dependence. *Journal of Geophysical Research: Atmosphere*, *118*(2), 547–562. https://doi.org/10.1002/jgrd.50153

Bromwich, D. H., Nicolas, J. P., Hines, K. M., Kay, J. E., Key, E. L., Lazzara, M. A., et al. (2012). Tropospheric clouds in Antarctica. *Reviews of Geophysics*, *50*(1), RG1004. https://doi.org/10.1029/2011RG000363

Caldwell, P. M., Zelinka, M. D., Taylor, K. E., & Marvel, K. D. (2016). Quantifying the sources of intermodel spread in equilibrium climate sensitivity. *Journal of Climate*, *29*(2), 513–524. https://doi.org/10.1175/JCLI-D-15-0352.1

Ceppi, P., Hwang, Y. T., Frierson, D. M. W., & Hartmann, D. L. (2012). Southern Hemisphere jet latitude biases in CMIP5 models linked to shortwave cloud forcing. *Geophysical Research Letters*, *39*, L19708. https://doi.org/10.1029/2012GL053115

Collins, M., Knutti, R., Arblaster, J. M., Dufresne, J.-L., Fichefet, T., Friedlingstein, P., et al. (2013). Long-term Climate Change: Projections, Commitments and Irreversibility. *Climate Change 2013: The physical science basis. Contribution of working group I to the fifth assessment report of the intergovernmental panel on climate change*. 1029–1136. Cambridge University Press. https://doi.org/10.1017/CBO9781107415324.024

Compo, G. P., Whitaker, J. S., Sardeshmukh, P. D., Matsui, N., Allan, R. J., Yin, X., et al. (2011). The twentieth century reanalysis project. *Quarterly Journal of the Royal Meteorological Society*, *137*(654), 1–28. https://doi.org/10.1002/qj.776

Curtis, P. E., Ceppi, P., & Zappa, G. (2020). Role of the mean state for the southern hemispheric jet stream response to CO_2 forcing in CMIP6 models. *Environmental Research Letters*, *15*, 064011. https://doi.org/10.1088/1748-9326/ab8331

Flato, G. M., Marotzke, J., Abiodun, B., Braconnot, P., Chou, S. C., Collins, W. J., & Cox, P. M. (2013). Evaluation of Climate Models. In *Climate Change 2013: The physical science basis .Contribution of working group I to the fifth assessment report of the intergovernmental panel on climate change* (pp. 741–866)

Forster, P. M., Andrews, T., Good, P., Gregory, J. M., Jackson, L. S., & Zelinka, M. D. (2013). Evaluating adjusted forcing and model spread for historical and future scenarios in the CMIP5 generation of climate models. *Journal of Geophysical Research Atmospheres*, *118*(3), 1139–1150. https://doi.org/10.1002/jgrd.50174

Frey, W. R., Morrison, A. L., Kay, J. E., Guzman, R., & Chepfer, H. (2018). The combined influence of observed Southern Ocean clouds and sea ice on top-of-atmosphere Albedo. *Journal of Geophysical Research: Atmosphere*, *123*(9), 4461–4475. https://doi.org/10.1029/2018JD028505

Frölicher, T. L., Sarmiento, J. L., Paynter, D. J., Dunne, J. P., Krasting, J. P., & Winton, M. (2015). Dominance of the Southern Ocean in anthropogenic carbon and heat uptake in CMIP5 models. *Journal of Climate*, *28*(2), 862–886. https://doi.org/10.1175/JCLI-D-14-00117.1

Goyal, R., Sen Gupta, A., Jucker, M., & England, M. H. (2021). Historical and projected changes in the southern hemisphere surface westerlies. *Geophysical Research Letters*, *48*, e2020GL090849. https://doi.org/10.1029/2020gl090849

Grise, K. M., & Medeiros, B. (2016). Understanding the varied influence of midlatitude jet position on clouds and cloud radiative effects in observations and global climate models. *Journal of Climate*, *29*(24), 9005–9025. https://doi.org/10.1175/JCLI-D-16-0295.1

Grise, K. M., Polvani, L. M., & Fasullo, J. T. (2015). Reexamining the relationship between climate sensitivity and the Southern Hemisphere radiation budget in CMIP models. *Journal of Climate*, *28*(23), 9298–9312. https://doi.org/10.1175/JCLI-D-15-0031.1

Hall, A., Cox, P. M., Huntingford, C., & Klein, S. (2019). Progressing emergent constraints on future climate change. *Nature Climate Change*, *9*(4), 269–278. https://doi.org/10.1038/s41558-019-0436-6

Hawkins, E., & Sutton, R. T. (2016). Connecting climate model projections of global temperature change with the real world. *Bulletin of the American Meteorological Society*, *97*(6), 963–980. https://doi.org/10.1175/BAMS-D-14-00154.2

Hyder, P., Edwards, J. M., Allan, R. P., Hewitt, H. T., Bracegirdle, T. J., Gregory, J. M., et al. (2018). Critical Southern Ocean climate model biases traced to atmospheric model cloud errors. *Nature Communications*, *9*(1), 3625. https://doi.org/10.1038/s41467-018-05634-2

Kidston, J., & Gerber, E. P. (2010). Intermodel variability of the poleward shift of the austral jet stream in the CMIP3 integrations linked to biases in 20th century climatology. *Geophysical Research Letters*, *37*(9), L09708. https://doi.org/10.1029/2010GL042873

Kidston, J., Taschetto, A. S., Thompson, D. W. J., & England, M. H. (2011). The influence of Southern Hemisphere sea-ice extent on the latitude of the mid-latitude jet stream. *Geophysical Research Letters*, *38*(15), L15804. https://doi.org/10.1029/2011GL048056

Klein, S. A., & Hartmann, D. L. (1993). The seasonal cycle of low stratiform clouds. *Journal of Climate*, *6*, 1587–1606. https://doi.org/10.1175/1520-0442(1993)006<1587:tscols>2.0.co;2

Lyu, K., Zhang, X., & Church, J. A. (2020). Regional dynamic sea level simulated in the CMIP5 and CMIP6 models: Mean biases, future projections, and their linkages. *Journal of Climate*, *33*(15), 6377–6398. https://doi.org/10.1175/jcli-d-19-1029.1

Manabe, S., Stouffer, R. J., Spelman, M. J., & Bryan, K. (1991). Transient responses of a coupled ocean--atmosphere model to gradual changes of atmospheric CO_2. Part I. Annual mean response. *Journal of Climate*, *4*(8), 785–818. https://doi.org/10.1175/1520-0442(1991)004<0785:troaco>2.0.co;2

Marshall, J., & Speer, K. (2012). Closure of the meridional overturning circulation through Southern Ocean upwelling. *Nature Geoscience*, *5*(3), 171–180. https://doi.org/10.1038/ngeo1391

Meehl, G. A., Washington, W. M., Arblaster, J. M., Hu, A., Teng, H., Kay, J. E., et al. (2013). Climate change projections in CESM1(CAM5) compared to CCSM4. *Journal of Climate*, *26*(17), 6287–6308. https://doi.org/10.1175/JCLI-D-12-00572.1

Mikaloff Fletcher, S. E., Gruber, N., Jacobson, A. R., Doney, S. C., Dutkiewicz, S., Gerber, M., et al. (2006). Inverse estimates of anthropogenic CO_2 uptake, transport, and storage by the ocean. *Global Biogeochemical Cycles*, *20*(2), a–n. https://doi.org/10.1029/2005GB002530

Miller, R. L., Schmidt, G. A., & Shindell, D. T. (2006). Forced annular variations in the 20th century intergovernmental panel on climate change fourth assessment report models. *Journal of Geophysical Research*, *111*(18), D18101. https://doi.org/10.1029/2005JD006323

Nohara, D., Tsutsui, J., Watanabe, S., Tachiiri, K., Hajima, T., Okajima, H., & Matsuno, T. (2015). Examination of a climate stabilization pathway via zero-emissions using Earth system models.*Environmental Research Letters*,*10*, 095005. https://doi.org/10.1088/1748-9326/10/9/095005

O'Neill, B. C., Tebaldi, C., Van Vuuren, D. P., Eyring, V., Friedlingstein, P., Hurtt, G., et al. (2016). The scenario model intercomparison project (ScenarioMIP) for CMIP6. *Geoscientific Model Development*, *9*(9), 3461–3482. https://doi.org/10.5194/gmd-9-3461-2016

Priestley, M. D. K., Ackerley, D., Catto, J. L., Hodges, K. I., McDonald, R. E., & Lee, R. W. (2020). An overview of the extratropical storm tracks in CMIP6. *Journal of Climate*, *33*, 6315–6343. https://doi.org/10.1175/JCLI-D-19-0928.1

Roach, L. A., Dörr, J., Holmes, C. R., Massonnet, F., Blockley, E. W., Notz, D., et al. (2020). Antarctic Sea ice area in CMIP6. *Geophysical Research Letters*, *47*, e2019GL086729. https://doi.org/10.1029/2019GL086729

Sarmiento, J. L., Gruber, N., Brzezinski, M. A., & Dunne, J. P. (2004). High-latitude controls of thermocline nutrients and low latitude biological productivity. *Nature*, *427*(6969), 56–60. https://doi.org/10.1038/nature02127

Seland, Ø., Bentsen, M., Seland Graff, L., Olivié, D., Toniazzo, T., Gjermundsen, A., et al. (2020). The Norwegian Earth System Model, NorESM2 – Evaluation of theCMIP6 DECK and historical simulations.*Geoscientific Model Development Discussions*, (February). https://doi.org/10.5194/gmd-2019-378

Sherwood, S., Webb, M. J., Annan, J. D., Armour, K. C., Forster, P. M., Hargreaves, J. C., et al. (2020). An assessment of Earth's climate sensitivity using multiple lines of evidence. *Reviews of Geophysics*, *58*. e2019RG000678. https://doi.org/10.1029/2019RG000678

Simpson, I. R., & Polvani, L. M. (2016). Revisiting the relationship between jet position, forced response, and annular mode variability in the southern midlatitudes. *Geophysical Research Letters*, *43*(6), 2896–2903. https://doi.org/10.1002/2016GL067989

Stocker, T. F., Qin, D., Plattner, G.-K., Tignor, M., Allen, S. K., Boschung, J., et al. (2013). *Climate change 2013: The physical science basis. Contribution of working group I to the fifth assessment report of the intergovernmental panel on climate change*. Cambridge university press Cambridge.

Thackeray, C. W., & Hall, A. (2019). An emergent constraint on future Arctic sea-ice albedo feedback. *Nature Climate Change*, *9*(12), 972–978. https://doi.org/10.1038/s41558-019-0619-1

Toggweiler, J. R., & Samuels, B. (1995). Effect of Drake Passage on the global thermohaline circulation. *Deep Sea Research Part I: Oceanographic Research Papers*, *42*(4), 477–500. https://doi.org/10.1016/0967-0637(95)00012-u

Tokarska, K. B., Stolpe, M. B., Sippel, S., Fischer, E. M., Smith, C. J., Lehner, F., & Knutti, R. (2020). Past warming trend constrains future warming in CMIP6 models. *Science Advances*, *6*(March), eaaz9549. https://doi.org/10.1126/sciadv.aaz9549

Trenberth, K. E., & Fasullo, J. T. (2010). Simulation of present-day and twenty-first-century energy budgets of the southern oceans. *Journal of Climate*, *23*(2), 440–454. https://doi.org/10.1175/2009JCLI3152.1

Wall, C. J., Hartmann, D. L., & Ma, P.-L. (2017). Instantaneous linkages between clouds and large-scale meteorology over the Southern Ocean in observations and a climate model. *Journal of Climate*, *30*(23), 9455–9474. https://doi.org/10.1175/JCLI-D-17-0156.1

Wild, M. (2020). The global energy balance as represented in CMIP6 climate models. *Climate Dynamics*, *55*, 553–577. https://doi.org/10.1007/s00382-020-05282-7

Williams, K. D., Copsey, D., Blockley, E. W., Bodas-Salcedo, A., Calvert, D., Comer, R., et al. (2017). The met office global coupled model 3.0 and 3.1 (GC3.0 and GC3.1) configurations. *Journal of Advances in Modeling Earth Systems*, *10*(2), 357–380. https://doi.org/10.1002/2017MS001115

Xie, S.-P., Deser, C., Vecchi, G. A., Ma, J., Teng, H., & Wittenberg, A. T. (2010). Global warming pattern formation: Sea surface temperature and rainfall. *Journal of Climate*, *23*(4), 966–986. https://doi.org/10.1175/2009JCLI3329.1

Zelinka, M. D., Myers, T. A., McCoy, D. T., Po-Chedley, S., Caldwell, P. M., Ceppi, P., et al. (2020). Causes of higher climate sensitivity in CMIP6 models. *Geophysical Research Letters*, *47*, e2019GL085782. https://doi.org/10.1029/2019GL085782

Zhai, C., Jiang, J. H., & Su, H. (2015). Long-term cloud change imprinted in seasonal cloud variation: More evidence of high climate sensitivity. *Geophysical Research Letters*, *42*(20), 8729–8737. https://doi.org/10.1002/2015GL065911

Zhu, J., & Poulsen, C. J. (2020). On the increase of climate sensitivity and cloud feedback with warming in the Community Atmosphere Models. *Geophysical Research Letters*, *47*, e2020GL089143. https://doi.org/10.1029/2020GL089143